The Genetic Architecture of Arabidopsis thaliana in Response to Native Non-Pathogenic Bacterial Species Revealed by Genome-Wide Association Mapping in Field Conditions

Daniela Ramírez-Sánchez, Rémi Duflos, Chrystel Gibelin-Viala, Rémy Zamar, Fabienne Vailleau, Fabrice Roux

OPEN ACCESS
phytobiomesjournal.org
Phytobiomes Journal
A Transdisciplinary Journal of Sustainable Plant Productivity

RESEARCH

The Genetic Architecture of *Arabidopsis thaliana* in Response to Native Non-Pathogenic Bacterial Species Revealed by Genome-Wide Association Mapping in Field Conditions

Daniela Ramírez-Sánchez, Rémi Duflos, Chrystel Gibelin-Viala, Rémy Zamar, Fabienne Vailleau, and Fabrice Roux†

LIPME, INRAE, CNRS, Université de Toulouse, Castanet-Tolosan, France

Accepted for publication 7 May 2024.

ABSTRACT

Non-pathogenic bacteria can substantially contribute to plant health by mobilizing and supplying nutrients, providing protection against pathogens, and alleviating abiotic stresses. However, the number of genome-wide association studies reporting the genetic architecture of the response to individual members of the beneficial microbiota remains limited. In this study, we established a genome-wide association study under field conditions to estimate the level of genetic variation and the underlying genetic architecture among 162 accessions of *Arabidopsis thaliana* originating from 54 natural populations in the southwest of France in response to 13 strains of seven of the most abundant and prevalent non-pathogenic bacterial species isolated from the leaf compartment of *A. thaliana* in the same geographical region. Using a high-throughput phenotyping methodology to score vegetative growth-related traits, extensive genetic variation was detected among *A. thaliana* accessions in response to these leaf bacteria, at both the species and strain levels. The presence of crossing reaction norms between each strain and the mock treatment indicates that declaring a strain as a plant growth-promoting bacterium is highly dependent on the host genotype tested. In line with the strong genotype-by-genotype interactions, we detected a complex and highly flexible genetic architecture between the 13 strains. Finally, the candidate genes underlying the quantitative trait loci revealed significant enrichment in several biological pathways, including cell, secondary metabolism, signaling, and transport. Altogether, plant innate immunity appears as a significant source of natural genetic variation in plant–microbiota interactions and opens new avenues for better understanding the ecologically relevant molecular dialog during plant–microbiota interactions.

Keywords: association genetics, microbiota, natural populations, plant growth-promoting bacteria, plant immunity

Both wild plant species and crops are consistently challenged by pathogens, making infectious disease often the major selective agent in nature (Burdon and Zhan 2020; Jeger 2022). In wild species, pathogen attacks can significantly decrease the number of offspring, which in turn affects the population growth rate of the host (Roux and Frachon 2022; Zhan et al. 2022). Yield losses resulting from pathogen attacks can reach several tens of percent in crops (Savary et al. 2019), thereby threatening global food security (Ristaino et al. 2021; Savary et al. 2019). A major challenge in ecological genomics and plant breeding is therefore to characterize the genetic architecture of response to pathogen attacks (Bartoli and Roux 2017). Identifying the genetic and molecular bases for natural variation in response to pathogen attacks might lead to fundamental insights in the prediction of evolutionary trajectories of natural populations (Burdon et al. 2006; Karasov et al. 2014) and have enormous practical implications by increasing crop yield and quality (Deng et al. 2020).

Over the last decade, whole-genome sequencing made possible through the development of cutting-edge next-generation sequencing technologies, combined with the development of increasingly sophisticated statistical methods in quantitative genetics (Bergelson and Roux 2010), has led to a burst in the number of genome-wide association studies (GWASs) in both wild and cultivated plants (Demirjian et al. 2023b). This allowed for the detection of genomic regions associated with natural variation of response to experimen-

†Corresponding author: F. Roux; fabrice.roux@inrae.fr

D. Ramírez-Sánchez and R. Duflos contributed equally to this work and share first authorship.

F. Vailleau and F. Roux share senior authorship.

Funding: D. Ramírez-Sánchez was funded by a Ph.D. fellowship from CONACYT (No. 707943). R. Duflos was funded by a grant from the French Ministry of National Education and Research. This project has received funding from the European Research Council (ERC) under the European Union's Horizon 2020 research and innovation program (grant agreement 951444 –PATHOCOM). This study was performed at the Laboratoire des Interactions Plantes-Microbes-Environnement belonging to the Laboratoire d'Excellence TULIP (ANR-10-LABX-41).

e-Xtra: Supplementary material is available online.

The author(s) declare no conflict of interest.

tal inoculation with, in most cases, individual pathogenic strains (Bartoli and Roux 2017; Gupta et al. 2019). GWASs revealed that the genetic architecture of plant response to pathogen attacks was highly polygenic (Bartoli and Roux 2017), highly dependent on the abiotic environment (Aoun et al. 2017, 2020), and dynamic along the infection stages (Aoun et al. 2020; Demirjian et al. 2022, 2023a). In addition, the functional validation of a few quantitative trait loci (QTLs) combined with transcriptomic analyses revealed the involvement of a broad range of rarely considered molecular functions in plant immunity (Badet et al. 2017; Debieu et al. 2016; Roux et al. 2014) and new defense pathways (Delplace et al. 2020).

However, the entire set of microbial pathogens—also called pathobiota—represents only a small fraction of the entire set of microbes inhabiting plants, the so-called plant microbiota. For instance, in the leaf compartment of 163 natural populations of *Arabidopsis thaliana* in the southwest of France and characterized for bacterial communities using a metabarcoding approach allowing for distinguishing pathogenic bacteria from other bacterial species (Bartoli et al. 2018), the relative abundance of pathobiota in microbiota was on average 1.6% in asymptomatic plants and 4.5% in plants with visible disease symptoms (Bartoli et al. 2018). Furthermore, microbiota can substantially contribute to plant health by (i) providing direct (e.g., production of antimicrobial components, niche competition) or indirect (e.g., triggering of immune defenses) protection against pathogens, (ii) mobilizing and provisioning nutrients to the plants, and (iii) alleviating abiotic stresses (such as drought) (Bai et al. 2022; Naitam et al. 2021; Trivedi et al. 2020). However, the number of GWASs reporting the genetic architecture of the response to experimental inoculation with individual members of the beneficial microbiota remains limited in comparison with the number of GWASs on the response to pathogens (Duflos et al. 2024). In addition, even though the phyllosphere represents 60% of the total biomass on Earth and concentrates 10^{26} bacteria (Vorholt 2012), most GWASs on the response to non-pathogenic bacteria focused on symbiotic bacteria or non-symbiotic plant growth-promoting bacteria (PGPBs) isolated from the belowground level and were conducted in laboratory controlled conditions (Cotta et al. 2020; Curtin et al. 2017; Stanton-Geddes et al. 2013; Torkamaneh et al. 2020; Vidotti et al. 2019; Wintermans et al. 2016).

In this study, we established a GWAS in field conditions to estimate the level of genetic variation and the underlying genetic architecture among 162 whole-genome sequenced accessions of *A. thaliana* originating from 54 natural populations in the southwest of France in response to 13 strains of seven of the most abundant and prevalent bacterial species isolated from the leaf compartment of *A. thaliana* in the same geographical region (Ramírez-Sánchez et al. 2022). We first developed a high-throughput phenotyping methodology to score vegetative growth-related traits on tens of thousands of plants. We then combined genome-wide association (GWA) mapping derived from a Bayesian hierarchical model with a local score approach to fine-map QTLs down to the gene level. We finally identified the main biological pathways associated with all the candidate genes and discuss the function of the main candidate genes that appear to matter in ecologically realistic conditions.

MATERIALS AND METHODS

Plant material. A total of 54 populations (each represented by three accessions randomly selected among, on average, 15 accessions per population) were chosen to represent both the genomic and ecological diversity identified among a set of 168 natural populations of *A. thaliana* located in the southwest of France (Bartoli et al. 2018; Frachon et al. 2018, 2019) (Supplementary Table S1). Seeds from maternal plants sampled in natural populations were collected in June 2016. Differences in the maternal effects among the 162 seed lots (54 populations × 3 accessions) were reduced by growing one plant of each accession for one generation (Supplementary Text).

Bacterial material. We considered two strains of 7 (i.e., OTU2, OTU3, OTU4, OTU5, OTU6, OTU13, and OTU29) out of the 12 most abundant and prevalent non-pathogenic leaf bacterial operational taxonomic units (OTUs) identified across 163 of the 168 natural populations of *A. thaliana* (Bartoli et al. 2018), except for OTU4, for which only one strain was available (Ramírez-Sánchez et al. 2022). These 12 OTUs were chosen according two criteria: (i) presence in more than 5% of 821 rosettes ($n > 41$) collected in situ in autumn 2014 and spring 2015 in the 163 natural populations of *A. thaliana* and characterized for bacterial communities by a metabarcoding approach based on a portion of the *gyrB* gene, which allows for a deeper taxonomic classification than the 16S rRNA gene (Bartoli et al. 2018), and (ii) OTUs with a mean relative abundance across all rosettes above 0.7% (Ramírez-Sánchez et al. 2022). Despite the use of two complementary approaches (i.e., community-based culture approach and information-driven approach), the use of several growth media, and the design of specific *gyrB*-based primers, we successfully isolated strains for only 7 of the 12 OTUs (Ramírez-Sánchez et al. 2022).

By combining de novo whole-genome sequencing of the 13 selected strains using the long-read sequencing PacBio technology and average nucleotide identity-based genomic taxonomic classification (Ramírez-Sánchez et al. 2022), OTU2, OTU5, and OTU6 were taxonomically classified at the species level as *Paraburkholderia fungorum*, *Pseudomonas moraviensis*, and *Pseudomonas siliginis*, respectively (Ramírez-Sánchez et al. 2022). OTU13 was taxonomically classified at the genus level as a *Methylobacterium* sp., whereas OTU3, OTU4, and OTU29 were taxonomically classified at the family level as an *Oxalobacteraceae* bacterium, *Comamonadaceae* bacterium, and *Sphingomonadaceae* bacterium, respectively (Ramírez-Sánchez et al. 2022). The 13 bacterial strains considered in this study were stored in a 20% glycerol solution at –80°C.

For the purpose of another study, we also included the strain JACO-CL of the bacterial pathogen *Pseudomonas viridiflava* (OTU8) (Bartoli et al. 2024), which is the second most abundant and prevalent bacterial pathogen across the 163 natural populations of *A. thaliana* (Bartoli et al. 2018).

Experimental design and growth conditions. A field experiment was set up at the INRAE center of Auzeville-Tolosane using a split-plot design arranged as a randomized complete block design with 16 treatments nested within six experimental blocks (Supplementary Fig. S1). The 16 treatments correspond to two mock treatments and the individual inoculation of 14 bacterial strains, namely OTU2_*Pfu*_1, OTU2_*Pfu*_2, OTU3a_*Oxa*_1, OTU3a_*Oxa*_2, OTU4_*Com*_1, OTU5_*Pmo*_1, OTU5_*Pmo*_2, OTU6_*Psi*_1, OTU6_*Psi*_2, OTU13_*M*sp_1, OTU13_*M*sp_2, OTU29_*Sph*_1, OTU29_*Sph*_2, and OTU8_JACO-CL. Each block was represented by 48 trays of 54 individual bottom-pierced wells (Ø4.7 cm, vol. ~70 cm²) (SOPARCO, reference 4920) filled with the potting soil PROVEEN Semi-Bouturage 2. In each block, each treatment corresponded to three trays stuck to each other and containing 162 plants, with one replicate per accession (54 populations × 3 accessions). In total, our experiment consisted of 15,552 plants (6 blocks × 16 treatments × 162 plants per block).

Randomization of accessions was kept identical among treatments within a block but differed among the six blocks. Randomization of the 16 treatments differed between the six blocks, except for the two mock treatments that were kept at the same position (Supplementary Fig. S1).

All seeds were sown on 18 March 2021, with several seeds sown in each well. Two weeks after sowing, seedlings were thinned to one per well, keeping the seedling the closest to the center of the well. During the entire growing period, the plants were watered as needed (i.e., no watering on rainy days and manual watering with a water mist spray gun every morning and every evening on hot and dry days until the potting soil was saturated with water). The amount of water applied strongly varied according to the weather. A molluscicide (Algoflash Naturasol) was regularly applied around the trays.

Inoculation procedure. Bacterial strains were grown on solid medium in Petri dishes (TSA for OTU5, OTU6, and OTU8; TSB for OTU2; R2A for OTU3, OTU4, OTU13, and OTU29). On the day of inoculation, bacterial colonies were resuspended in sterile deionized water, and bacterial solutions were diluted to reach an $OD_{600\ nm}$ of 0.01. To facilitate the penetration of bacteria cells into plant organs, the Tween 20 surfactant was added to each bacterial solution at a final concentration of 0.01%. Inoculation was performed 27 days after sowing (14 Apri 2021), when most plants reached the five- to six-leaf stage. Using a Multipette multi-dispenser pipette with a 50-ml Combitips advanced dispenser tip, a volume of 1 ml of inoculum was dispensed on each rosette. A volume of 1 ml of sterile water with a Tween concentration of 0.01% was dispensed on each rosette of the plants of the two mock treatments. To increase relative humidity, plants were watered with a water mist spray gun for 7 days following the inoculation.

Phenotyping. Following Roux et al. (2016), a nondestructive imaging approach (Supplementary Fig. S2) was used to measure each plant for nine traits related to vegetative growth (Supplementary Data Set 1): projected rosette surface area measured at 1 day before inoculation (dbi) (area-1dbi), 5 days after inoculation (dai) (area-5dai), and 9 dai (area-9dai); rosette perimeter measured at 1 dbi (perimeter-1dbi), 5 dai (perimeter-5dai), and 9 dai (perimeter-9dai); and maximal rosette diameter measured at 1 dbi (diameter-1dbi), 5 dai (diameter-5dai), and 9 dai (diameter-9dai). To estimate plant growth relative to size, three relative growth rates (RGRs) were estimated based on the rosette surface area: RGR between 5 dai and 1 dbi (RGR-5dai-1dbi), RGR between 9 and 5 dai (RGR-9dai-5dai), and RGR between 9 dai and 1 dbi (RGR-9dai-1dbi). The procedure and methodologies (including a high-throughput imaging-based phenotyping methodology) are detailed in the Supplementary Text.

Analysis of the extent of natural genetic variation. For the purpose of this study, the strain JACO-CL (OTU8, *P. viridiflava*) was not considered in any data analysis.

To test for the homogeneity of plant growth across the field trial and the presence of genetic variation for the three vegetative growth-related traits measured before inoculation, data from the two mock treatments were pooled, and the following mixed model (PROC MIXED procedure in SAS v. 9.4, SAS Institute, Cary, NC, U.S.A.) was used:

$$\begin{aligned} Y_{ijklmn} &= \mu_{trait} + Block_i + Treatment_j + Block_i \times Treatment_j \\ &\quad + Population_k + Population_k \times Treatment_j \\ &\quad + Line_l\,(Tray_n) + Column_m\,(Tray_n) + \varepsilon_{ijklmn} \end{aligned} \quad \text{(Model 1)}$$

where Y is one of the three phenotypic traits measured before inoculation (i.e., area-1dbi, perimeter-1dbi, and diameter-1dbi), μ is the overall mean of the phenotypic data, *Block* accounts for differences in micro-environmental conditions among blocks, *Line*(*Tray*) and *Column*(*Tray*) account for differences in micro-environmental conditions within 54-well trays, *Treatment* tests for differences among the 14 treatments (i.e., mock treatment and 13 treatments with non-pathogenic bacterial strains), *Population* corresponds to the genetic differences among the 54 populations, *Population* × *Treatment* tests whether the rank among the 54 populations differs among the 14 treatments, and ε is the residual term.

Whereas the terms *Treatment* and *Population* × *Treatment* were not significant for the three traits scored at 1 dbi, we detected a highly significant *Population* effect (Supplementary Table S2), thereby indicating that the level of significant genetic variation observed among the 54 populations was homogeneous across the field trial before inoculation.

To estimate the natural genetic variation of the response of the 162 accessions nested within 54 populations to the 13 non-pathogenic bacterial strains, the following mixed model (PROC MIXED procedure in SAS v. 9.4, SAS Institute) was used for each of the 14 treatments:

$$\begin{aligned} Y_{ijklm} &= \mu_{trait} + Block_i + Population_j + Accession_k\,(Population_j) \\ &\quad + Line_l\,(Tray_n) + Column_m\,(Tray_n) + \varepsilon_{ijklmn} \end{aligned} \quad \text{(Model 2)}$$

where Y corresponds to one of the nine traits (area-5dai, area-9dai, perimeter-5dai, perimeter-9dai, diameter-5dai, diameter-9dai, RGR-5dai-1dbi, RGR-9dai-5dai, and RGR-9dai-1dbi). All the terms were identical to the ones described in Model 1, except for the *Accession* term, which accounts for mean genetic differences among the three accessions within populations.

For each of the 126 phenotypic trait and treatment combinations (i.e., 9 traits × 14 treatments), genotypic values of the 54 populations were estimated by calculating least-squares mean values of the *Population* term in the following linear model (function *lm* of the library *lme4* under the R environment):

$$\begin{aligned} Y_{ijkl} &= \mu_{trait} + Block_i + Population_j + Line_k\,(Tray_m) \\ &\quad + Column_l\,(Tray_m) + \varepsilon_{ijklm} \end{aligned} \quad \text{(Model 3)}$$

We then applied the function *lsmeans* (library *lsmeans* under the R environment) to Model 3. For each of the nine phenotypic traits, the estimated genotypic values (Supplementary Data Set 2) were then used to (i) compare phenotypic variation among the 14 treatments, (ii) estimate the level of *Population* × *Treatment* interactions by calculating pairwise non-linear correlation coefficients (Spearman's *rho*) among the 14 treatments, and (iii) run GWA analyses (see below).

In Models 1, 2, and 3, all factors were treated as fixed effects. For calculating F values, terms were tested over their appropriate denominators. A correction for the number of tests was performed to control for the false discovery rate at a nominal level of 5%.

To estimate broad-sense heritability values (H^2) for each of the 126 phenotypic trait and treatment combinations, we first ran the following linear mixed model (function *lmer* of the library *lme4* under the R environment):

$$\begin{aligned} Y_{ijkl} &= \mu_{trait} + Block_i + Accession_j + Line_k\,(Tray_m) \\ &\quad + Column_l\,(Tray_m) + \varepsilon_{ijklm} \end{aligned} \quad \text{(Model 4)}$$

with the *Block* and *Accession* factors treated as random effects. The percentage of phenotypic variance explained by the *Block* and *Accession* terms was then estimated by applying the function *varcorr* (library *lme4* under the R environment) to Model 4. Following Huard-Chauveau et al. (2013), H^2 values were estimated using the following formula:

$$H^2_{Trait} = \frac{VF}{VF + \frac{VR}{N}}$$

where VF corresponds to the genetic variance among the 162 accessions, VR is the residual variance, and N is the mean number of biological replicates per accession ($N = 6$ in this study).

Combining GWA mapping with a local score approach. Using a Pool-seq approach based on the individual DNA extraction of on average 15 plants per population, a representative picture of within-population genetic variation was previously obtained for the 168 natural populations of *A. thaliana* located in the southwest of France (Frachon et al. 2018), leading to the estimation of standardized allele frequencies corrected for the effect of population structure within each population for 1,638,649 single-nucleotide polymorphisms (SNPs) across the genome (Frachon et al. 2018). For this study, standardized population allele frequencies were retrieved for the 54 populations. Then, following Ramírez-Sánchez et al. (2023), for each of the 126 phenotypic trait and treatment combinations, a genome scan was first launched by estimating for each SNP Spearman's *rho* and associated *P* values between standardized allele frequencies and population genotypic values. Thereafter, to increase (i) the resolution in fine mapping genomic regions associated with genetic variation in response to bacterial strains and (ii) the identification of QTLs with small effects, we followed Aoun et al. (2020), Demirjian et al. (2022), and Ramírez-Sánchez et al. (2023) by implementing a local score approach (with a tuning parameter $\xi = 2$) on these *P* values. Finally, significant SNP-phenotype associations were identified by estimating a chromosome-wide significance threshold for each chromosome (Bonhomme et al. 2019).

Enrichment in biological processes. A custom script written under the *R* environment was used to retrieve the candidate genes underlying detected QTLs for each of the 126 phenotypic trait and treatment combinations. For each of the 14 treatments, we merged the lists of candidate genes of the nine phenotypic traits and removed duplicates. For each of the 13 treatments with a non-pathogenic bacterial strain, only candidate genes not found in the mock treatment were kept. To identify biological pathways significantly overrepresented ($P < 0.01$), each of the 14 resulting lists of unique candidate genes was submitted to the classification SuperViewer tool on the University of Toronto website (https://bar.utoronto.ca/ntools/cgi-bin/ntools_classification_superviewer.cgi) using the MAPMAN classification.

RESULTS

Genetic variation of *A. thaliana* in response to non-pathogenic bacterial strains in field conditions. In agreement with previous experiments conducted under in vitro conditions (Ramírez-Sánchez et al. 2022), no disease symptoms were observed in response to the 13 non-pathogenic strains in our field conditions. For each of the 14 treatments (mock treatment and 13 treatments with a non-pathogenic bacterial strain), highly significant genetic variation was detected among the 54 populations (Fig. 1; Supplementary Fig. S3; Supplementary Table S3) for each of the nine phenotypic traits. Across the 126 phenotypic trait and treatment combinations, the mean broad-sense heritability (H^2) estimate was 0.49 (median = 0.56, quantile 5% = 0.16, quantile 95% = 0.70), indicating that a nonnegligible fraction of phenotypic variance was explained by genetic variation among populations and accessions (Supplementary Table S4).

Significant phenotypic variation was observed among the 14 treatments for each phenotypic trait (Fig. 1; Supplementary Fig. S3). However, significant differences between the mock treatment and the response to any bacterial strain were only observed for three traits (i.e., area-9dai, diameter-9dai, and RGR-5dai-1dbi) (Fig. 1; Supplementary Fig. S3). For instance, the rosette area at 9 dai was on average bigger and smaller in response to OTU2_*Pfu*_1/OTU3a_*Oxa*_2 and OTU29_*Sph*_2 than in the mock treatment, respectively (Fig. 1A). The relative growth rate between 5 dai and 1 dbi was significantly higher in response to OTU5_*Pmo*_2 than in seven treatments, including the mock treatment (Fig. 1B).

More importantly, for each phenotypic trait, we observed a strong genetic variation among the 54 populations of *A. thaliana* in their response to each of the 13 non-pathogenic bacterial strains (Fig. 2; Supplementary Fig. S4), with (i) values of genetic correlations between the mock treatment and each treatment with a bacterial strain greatly deviating from 1 (Fig. 2; Supplementary Fig. S4) and (ii) the observation of strong crossing reaction norms between the mock treatment and each treatment with a bacterial strain (Fig. 3). In addition, the response of the 54 populations strongly

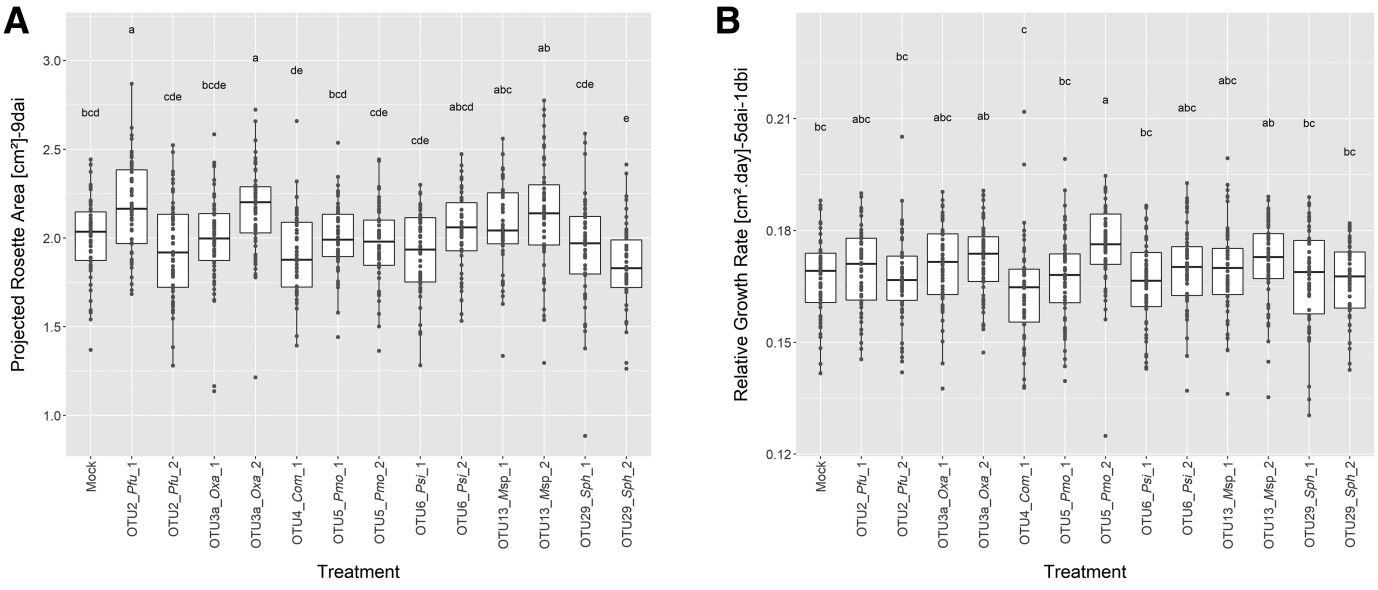

Fig. 1. Phenotypic variation of the response to the mock treatment and the 13 bacterial strains in field conditions. **A,** Boxplots illustrating the variation among the 14 treatments for the trait 'area-9dai'. **B,** Boxplots illustrating the variation among the 14 treatments for the trait 'RGR-5dai-1dbi'. For each treatment, each dot corresponds to the genotypic value of one of the 54 populations of *Arabidopsis thaliana*. For each trait, different letters indicate different groups according to the treatments after a Ryan-Einot-Gabriel-Welsh (REGWQ) multiple-range test at $P = 0.05$. dai: days after inoculation; dbi: days before inoculation; RGR: relative growth rate.

varied among the 13 bacterial strains, even between two strains belonging to the same bacterial species (Fig. 2; Supplementary Fig. S4). For instance, the direction and/or the strength of the response of a given population of *A. thaliana* could differ widely between the two OTU13_*M*sp strains, as illustrated by the FERR-A and LUZE-B populations (Fig. 3).

A genomic map of the response of *A. thaliana* to prevalent and/or abundant leaf bacterial species. Based on the allele frequencies of 1,638,649 SNPs obtained by a Pool-seq approach for each of the 54 populations (Frachon et al. 2018), a GWA mapping analysis combining a Bayesian hierarchical model with a local score approach was conducted to characterize the genetic architecture of the response to the 13 non-pathogenic bacterial strains. In line with the short linkage disequilibrium observed in natural populations of *A. thaliana* in France (Frachon et al. 2017), we detected 2,064 QTLs across the 126 phenotypic trait and treatment combinations, with a mean length of QTL interval equal to about 837 bp (quantile 5% $\sim$ 38 bp, quantile 95% $=$ 3.12 kb) (Supplementary Data Set 3). The number of QTLs per phenotypic trait and treatment combination ranged from 6 to 34 (mean $=$ 16.4), suggesting a polygenic architecture for the response of *A. thaliana* to members of the most prevalent and/or abundant non-pathogenic bacterial species of the leaf compartment of *A. thaliana* in the southwest of France (Fig. 4A).

In agreement with the level of genetic correlations observed among the 14 treatments and the presence of crossing reaction norms (Figs. 2 and 3; Supplementary Fig. S4), the genetic architecture was highly flexible (i) between the mock treatment and the treatments with a bacterial strain and (ii) among treatments with a bacterial strain at both the interspecific and intraspecific levels

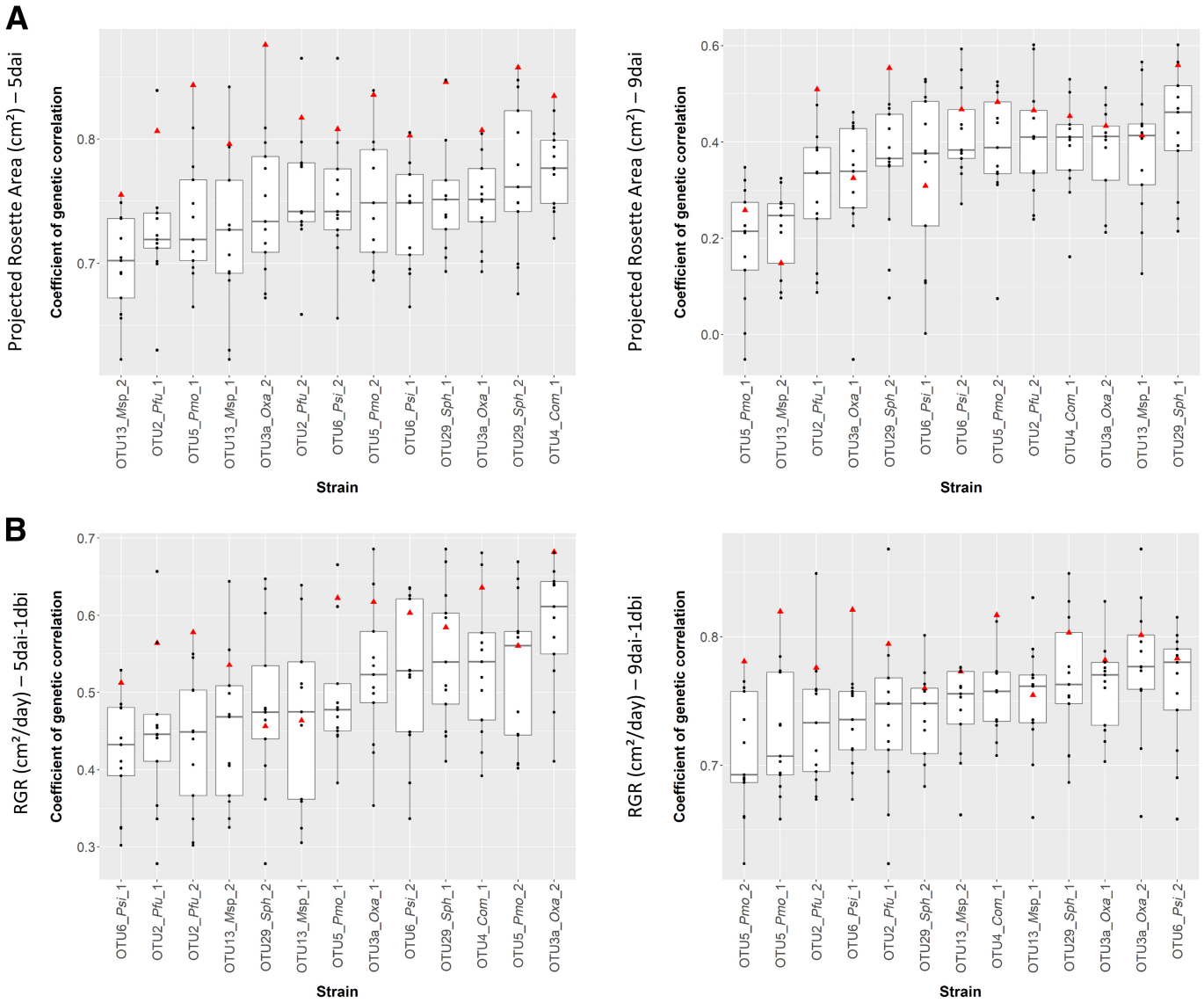

Fig. 2. Genetic variation of 54 natural populations of *Arabidopsis thaliana* in response to the 13 bacterial strains in field conditions. **A,** Boxplots illustrating the range of genetic correlations between each treatment with a bacterial strain and the remaining 13 treatments for the traits 'area-5dai' and 'area-9dai'. **B,** Boxplots illustrating the range of genetic correlations between each treatment with a bacterial strain and the remaining 13 treatments for the traits 'RGR-5dai-1dbi' and 'RGR-9dai-1dbi'. Red triangle: genetic correlation with the mock treatment; black dots: genetic correlations with other treatments with a bacterial strain. dai: days after inoculation; dbi: days before inoculation; RGR: relative growth rate. Treatments are ranked according to their mean genetic correlation with other treatments.

(Fig. 5). Most candidate genes underlying detected QTLs and not shared with the mock treatment were specific to a given treatment with a bacterial strain, in particular at 9 dai (Fig. 4B; Supplementary Fig. S5; Supplementary Data Set 4). For instance, for the maximal rosette diameter, whereas the percentage of candidate genes specific to a given treatment with a bacterial strain ranged from 57.7 to 86.1% (mean = 75.2%) at 9 dai, it ranged from 26.9 to 81.1% (mean = 46.0%) at 5 dai (Supplementary Fig. S5).

Identification of enriched biological processes and candidate genes associated with the response to prevalent and abundant leaf bacterial species. The first approach to identify relevant candidate genes involved in the response to the 13 non-pathogenic bacterial species was to focus on candidate genes underlying the most pleiotropic QTLs. Here, we focused on QTLs detected for the response to more than six bacterial strains but not detected for the mock treatment. We identified seven such pleiotropic QTLs encompassing 17 candidate genes (Fig. 6; Supplementary Data Set 5), among which eight genes have functions in relation to plant development and organ growth: *At2g40650* (Watanabe et al. 2019), *At2g40670* (Yang et al. 2020), *At2g44710* (Zhang et al. 2022), *At2g47190* (Guo et al. 2022), *At4g14713* (White 2022), *At4g14716* (Friedman et al. 2011), *At4g14720* (Baekelandt et al. 2018), and *At5g42360* (Franciosini et al. 2013). Interestingly, three genes have a link with plant immunity: *MEMB12* (*At5g50440*), which is silenced by a microRNA during *Pseudomonas syringae* bacterial infection (Chung et al. 2018); *ARR16* (*At2g40670*), which is repressed by *Botrytis cinerea* fungal infection (Li et al. 2021); and *TIFY4B/ PEAPOD2* (*At4g14720*), which interacts with the begomovirus AL2 transcriptional activator protein, an inhibitor of plant basal defense (Chung and Sunter 2014).

Based on the lists of unique candidate genes identified for each treatment and the list of unique candidate genes identified across the 13 treatments with a bacterial strain, the second approach was to identify biological processes significantly overrepresented in frequency compared with the overall class frequency in the *A. thaliana* MapMan annotation. When considering both the 14 treatments individually and the 13 treatments with a bacterial strain altogether, we identified 19 significantly enriched classes, among which five were enriched in the mock treatment (i.e., 'development', 'hormone metabolism', 'lipid metabolism', 'protein', and 'RNA') (Fig. 7A; Supplementary Data Set 5). Amongst the 14 overrepresented classes not detected in the mock treatment, most of them were highly dependent on the identity of the bacterial strain, suggesting the involvement of diverse pathways in response to representative members of the non-pathogenic microbiota, down to the intraspecific level (Fig. 7A). We nonetheless identified four classes that were significantly overrepresented for at least three treatments with a bacterial strain and when considering the 13 treatments with a bacterial strain altogether: 'cell', 'secondary metabolism', 'signaling', and 'transport' (Fig. 7A). Interestingly, in the set of the 99 'signaling' genes, we identified, among others, 54 kinase-related genes (including 24 leucine-rich repeat kinases, 8 cysteine-rich receptor-like kinases [CRKs], and 6 mitogen-activated protein kinases) and 23 genes associated with calcium signaling (Fig. 7B).

DISCUSSION

Extensive genetic variation within a regional set of *A. thaliana* accessions in response to non-pathogenic leaf bacteria at the species and strain levels. Extensive genetic variation was previously observed in two worldwide collections of *A. thaliana*, each challenged at the root level under in vitro conditions with a single PGPB strain isolated from a plant species other than *A. thaliana* (i.e., the strain *Pseudomonas simiae* WCS417r isolated from the rhizosphere of wheat [Wintermans et al. 2016] and the strain *Bacillus pumilus* TUAT-1 isolated from rice roots [Cotta et al. 2020]).

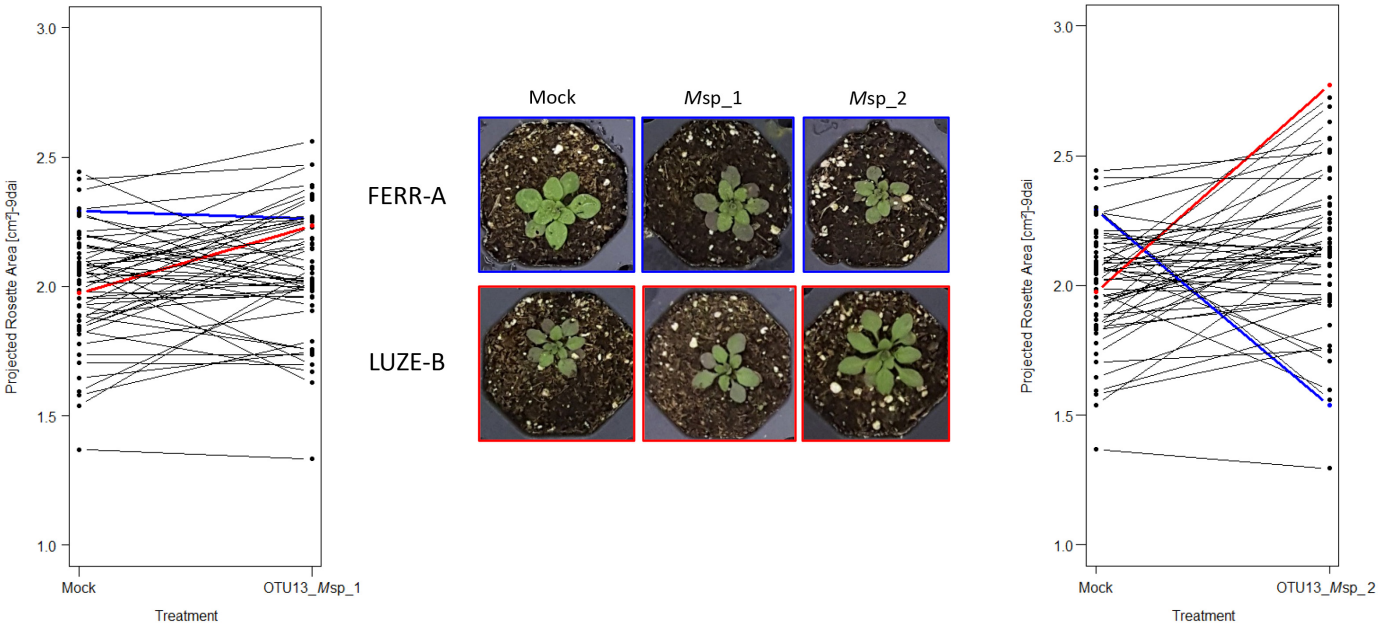

Fig. 3. Interaction plots illustrating the reaction norms observed at the population level between the mock treatment and the treatment with OTU13_*M*sp_1 (left panel) and OTU13_*M*sp_2 (right panel). Each dot corresponds to the genotypic value of one of the 54 populations of *Arabidopsis thaliana*. Each line corresponds to the response of one of the 54 populations to the inoculation with either OTU13_*M*sp strain. The blue and red lines correspond to two populations, FERR-A and LUZE-B, respectively, with an opposite response to the strain OTU13_*M*sp_2. Pictures illustrate representative plants of the two populations highlighted in blue and red for the mock treatment and the treatment with either OTU13_*M*sp strain.

In this study, the ecological realism of plant–microbiota interactions was increased by phenotyping in field conditions the rosette growth response of *A. thaliana* accessions collected in the southwest of France to non-pathogenic bacterial strains isolated from the leaf compartment of *A. thaliana* in the same geographical region.

In agreement with previous observations with bacterial pathogens (Bartoli and Roux 2017; Demirjian et al. 2023b; Wang et al. 2018), the extent of genetic variation in response to non-pathogenic bacterial strains was more dependent on the identity of the bacterial strain than the identity of the bacterial species. In addition, the presence of crossing reaction norms indicates that declaring a strain as a PGPB is highly dependent on the host genotype tested. Whether the host genotype-dependent plant growth-promoting effect of a particular strain on aboveground vegetative growth is also observed at the

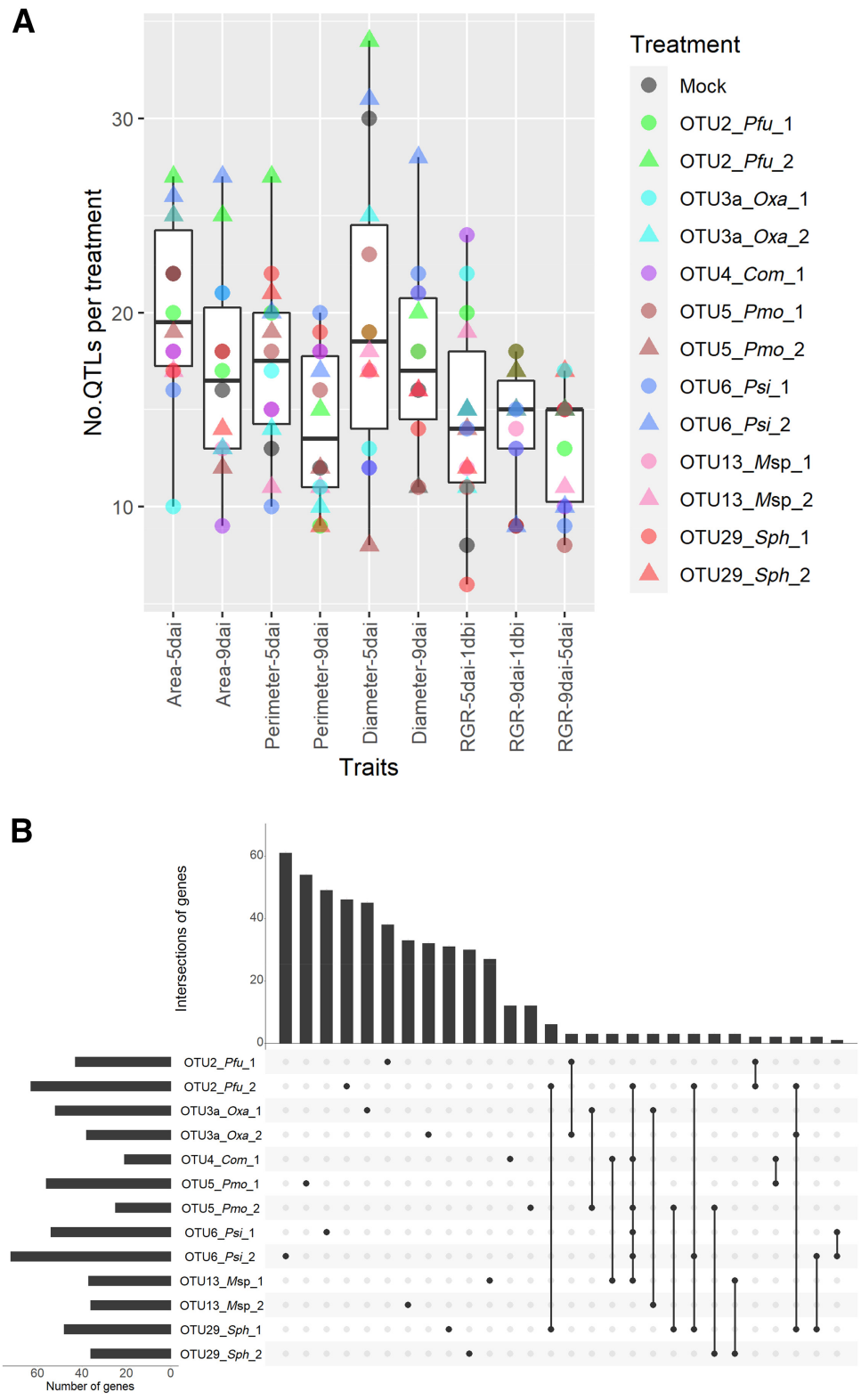

Fig. 4. Genetic architecture of the response of 54 natural populations of *Arabidopsis thaliana* to the 13 bacterial strains in field conditions. **A,** Number of quantitative trait loci (QTLs) per treatment for each of the nine phenotypic traits. **B,** An UpSet plot illustrating the flexibility of genetic architecture among the 13 treatments with bacterial strains for the trait 'area-9dai'. 'Number of genes': Total number of candidate genes underlying detected QTLs and not shared with the mock treatment. A single dot indicates the number of candidate genes specific to a given treatment. Candidate genes shared between two or more treatments are represented by a line connecting two or more dots. dai: days after inoculation.

belowground level would deserve investigation, for instance, by estimating root growth and root/shoot biomass ratios (Mantelin and Touraine 2004).

Interestingly, whereas genetic variation in response to bacterial strains was observed within a few days after inoculation in field conditions, such a genetic variation was mainly observed after several weeks under in vitro conditions (Ramírez-Sánchez et al. 2022). Because the bacterial strains used in this study were isolated from complex microbiota in the native habitats of *A. thaliana*, the effect of the bacterial strains may require the presence of additional microbiota members in the plant, a prerequisite not achieved in germ-free plants under in vitro conditions (Ramírez-Sánchez et al. 2022, 2023).

A complex and highly flexible genetic architecture underlies native plant–microbiota interactions. So far, the very few GWASs (Bergelson et al. 2021) and the single genome-environment association study (Roux et al. 2023) conducted on the leaf compartment and using bacterial community descriptors as phenotypic traits revealed a polygenic architecture controlling microbiota assembly, which is in line with the small percentage of variance explained

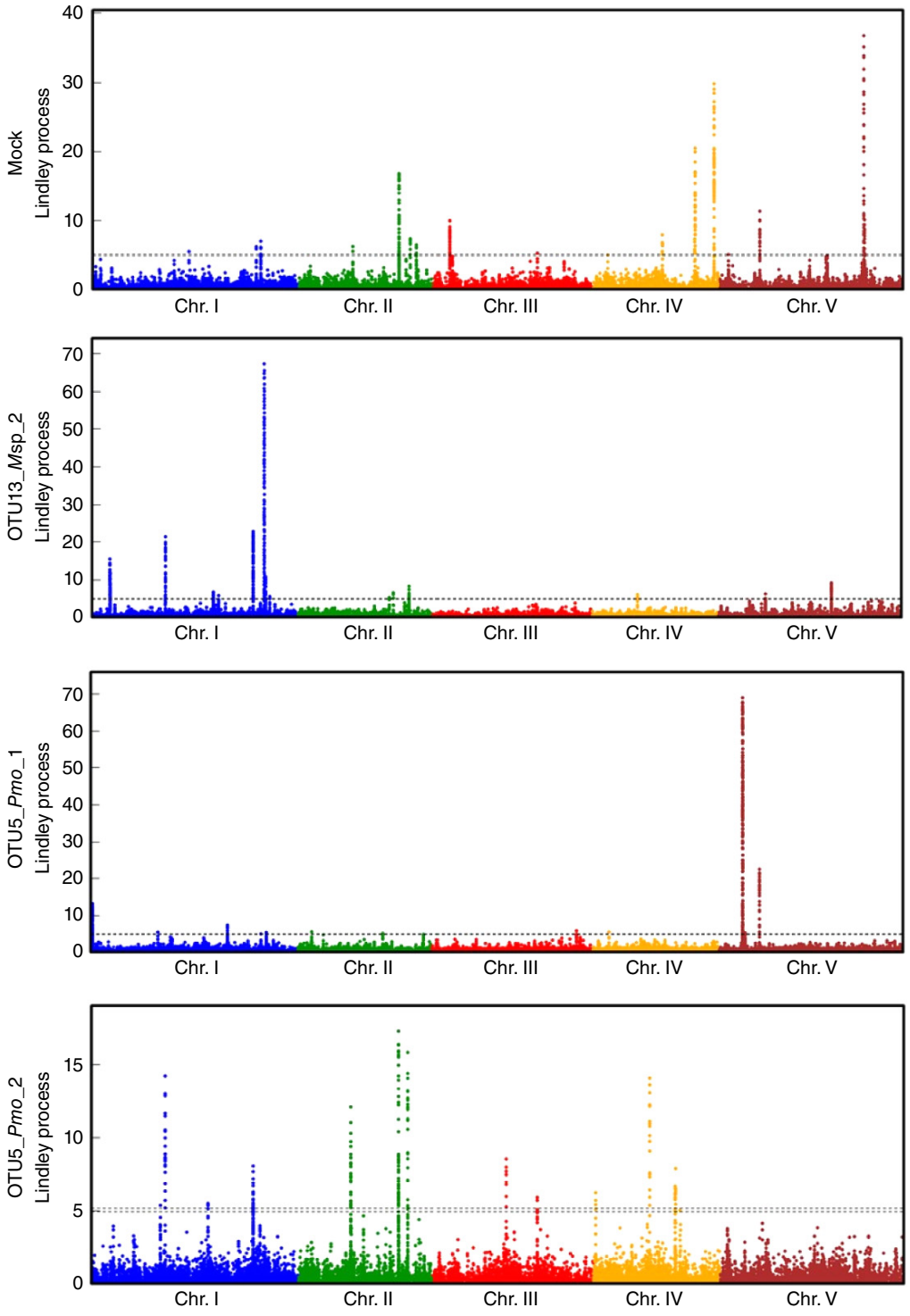

Fig. 5. Manhattan plots of the Lindley process for the trait 'area_9dai' for the mock treatment and the treatments with the bacterial strains OTU13_*M*sp_2, OTU5_*Pmo*_1, and OTU5_*Pmo*_2. The *x* axis corresponds to the physical position of 1,638,649 single-nucleotide polymorphisms on the five chromosomes of *A. thaliana*. The dashed lines indicate the minimum and maximum of the five chromosome-wide significance thresholds.

by the phenotyping of individual mutant lines (Bergelson et al. 2021). In agreement with these association genetic studies and the three GWASs conducted on *A. thaliana* in response to a PGPB strain (Cotta et al. 2020; Ramírez-Sánchez et al. 2023; Wintermans et al. 2016), we identified a complex genetic architecture for the response of *A. thaliana* to 13 non-pathogenic bacterial strains. In addition, this polygenic architecture was highly flexible among the 13 bacterial strains, with the detection of a small number of highly pleiotropic QTLs. Similar results were observed in recent GWASs conducted in both crops and wild species in response to experimental inoculation with individual pathogenic bacterial strains. For instance, challenging 130 natural accessions of *A. thaliana* with 22 strains of the bacterial pathogen *Xanthomonas arboricola* revealed a clear host-strain specificity in quantitative disease resistance (Wang et al. 2018). The complex genetic interactions observed between *A. thaliana* and the main members of its leaf microbiota should maintain a high level of diversity at the candidate genes, as previously observed in plant pathosystems (Karasov et al. 2014).

Plant innate immunity is a significant source of natural genetic variation in native plant–microbiota interactions. The candidate genes underlying the most pleiotropic QTLs have functions mainly related to plant development and/or stresses (biotic or abiotic stresses). Nevertheless, a more global approach identified four biological processes that were significantly and specifically overrepresented in response for at least three bacterial strains but not for the mock treatment (i.e., 'cell', 'secondary metabolism', 'signaling', and 'transport') (Fig. 7A). These four classes were also overrepresented in a genome-environment association study performed on 163 natural populations of *A. thaliana* located in the southwest of France (including the 54 populations considered in this study) (Roux et al. 2023) and characterized in situ for bacterial communities in the leaf and root compartments using a metabarcoding approach (Bartoli et al. 2018), thereby strengthening the importance of these four classes in mediating host response to the 13 bacterial strains tested here.

Strikingly, we found a strong enrichment for signaling genes underlying QTLs in response to the 13 bacterial strains tested in this study. Signaling genes have been extensively described as being involved in plant–microbe interactions. Of particular note, we identified eight genes belonging to the CRK family, which represents one of the largest groups of receptor-like kinases, with 44 members in *A. thaliana* (Bourdais et al. 2015). Some CRKs are involved in the regulation of plant developmental processes, whereas others are involved in stress and pathogen response (Bourdais et al. 2015). Interestingly, by assessing host transcriptional and metabolic adaptations to 39 bacterial strains in the leaf compartment of *A. thaliana*, a core set of 24 genes consistently induced by the presence of most strains was identified and thereby referred to as a molecular process called general non-self-response (Maier et al. 2021). Importantly, one gene of this core set (*CRK6*) was also identified as a candidate gene in our GWAs, reinforcing the importance of CRKs in plant–microbiota interactions.

In addition, we detected many candidate genes related to pattern-triggered immunity (PTI), including receptor-like kinases and receptor-like proteins. PTI relies on the perception of specific molecular patterns, such as microbe-associated molecular patterns (Macho and Zipfel 2014). In particular, we identified a main actor of PTI, the *FLS2* gene encoding a leucine-rich repeat receptor-like kinase protein that acts as a receptor for the flg22 bacterial pathogen-associated molecular pattern (Macho and Zipfel 2014), as a candidate gene in response to the two strains of OTU6 and one strain of OTU13 (Supplementary Data Set 6), which is in line with two recent studies that dissected the interplay between FLS2 and diverse flg22 variants from the bacterial microbiota of *A. thaliana* (Colaianni et al. 2021; Parys et al. 2021). Interestingly, PTI can be modulated by a physical association between FLS2 and CRK6 (Yeh et al. 2015). PTI response is also characterized by the production of reactive oxygen species and by the activation of the mitogen-activated protein kinase cascade (Monaghan and Zipfel 2012). In our study, we identified four NADPH oxidase *RBOH* genes, among

ATG number	Annotation	OTU2_*Pfu*_1	OTU2_*Pfu*_2	OTU3a_*Oxa*_1	OTU3a_*Oxa*_2	OTU4_*Com*_1	OTU5_*Pmo*_1	OTU5_*Pmo*_2	OTU6_*Psi*_1	OTU6_*Psi*_2	OTU13_*Msp*_1	OTU13_*Msp*_2	OTU29_*Sph*_1	OTU29_*Sph*_2
At2g40640	PUB62 (Plant U-box type E3 ubiquitin ligase)													
At2g40650	PRP38													
At2g40660	Nucleic acid-binding, OB-fold-like protein													
At2g40670	ARR16 (ARABIDOPSIS THALIANA RESPONSE REGULATOR 16)													
At2g44710	HNRNP R-LIKE PROTEIN, HRLP													
At2g44730	Alcohol dehydrogenase transcription factor Myb/SANT-like family protein													
At2g44735	transmembrane protein													
At2g47180	ATGOLS1, GALACTINOL SYNTHASE 1													
At2g47190	ATMYB2, MYB DOMAIN PROTEIN 2													
At2g47250	RNA helicase family protein													
At4g14713	PEAPOD 1, PPD1, TIFY4A													
At4g14716	ACIREDUCTONE DIOXYGENASE 1, ARD1, ATARD1, SGB3, SUPPRESSOR OF G BETA 3													
At4g14720	PEAPOD 2, PPD2, TIFY4B													
At5g42360	CFK2, COP9 SIGNALOSOME INTERACTING F-BOX KELCH 2													
At5g42370	Calcineurin-like metallo-phosphoesterase superfamily protein													
At5g50440	ATMEMB12, MEMB12, MEMBRIN 12													
At5g50450	HCP-like superfamily protein with MYND-type zinc finger													

Fig. 6. List of pleiotropic candidate genes associated with more than six treatments with a bacterial strain but not detected in the mock treatment. Colored squares indicate the strains for which the candidate genes were identified. The different colors correspond to the seven quantitative trait loci (QTLs) in which the pleiotropic QTLs are located.

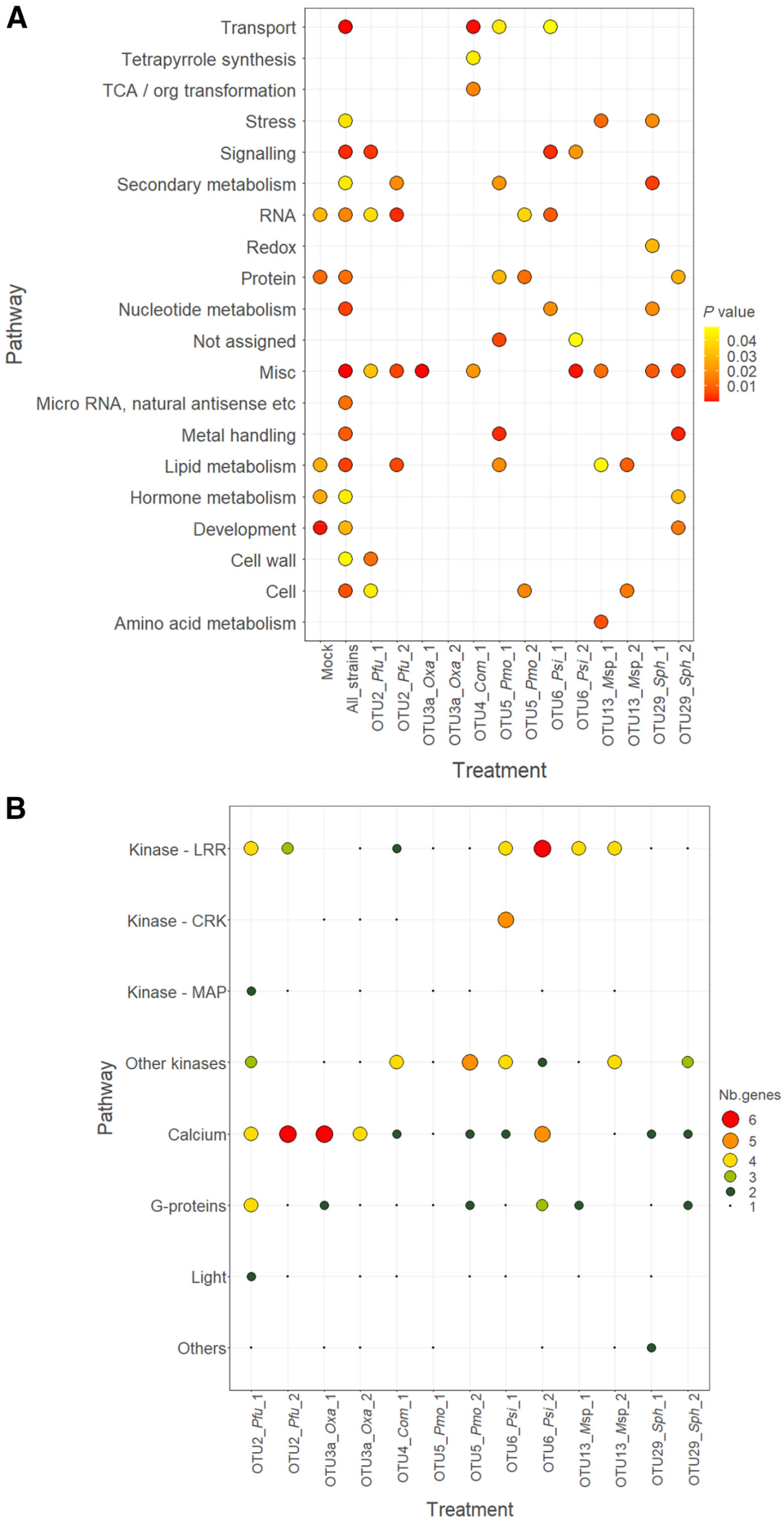

Fig. 7. Enriched biological processes in response to the 13 bacterial strains in field conditions. **A,** Enriched biological processes for the list of unique candidate genes for each of the 14 treatments and for the list of unique candidate genes from the combined 13 bacterial strains ('All strains'), obtained with the MapMan classification SuperViewer tool. The color of the dots corresponds to the level of significance. **B,** Number of candidate genes belonging to the different subcategories of the enriched 'signaling' biological process for each treatment with a bacterial strain. LRR: leucine-rich repeat; CRK: cysteine-rich receptor-like kinase; MAP: mitogen-activated protein.

them the gene *RBOHD* that is required for microbiota homeostasis in leaves (Pfeilmeier et al. 2021). Another candidate gene is *MPK4*, a main actor of PTI signaling (Bazin et al. 2020). Even if few mutant lines related to signaling and PTI have been tested for their effect on microbiota assembly (Bergelson et al. 2021), our results strengthen the need for a deeper investigation of some of our most promising candidate genes in relationship with the 13 strains used in this study. Importantly, the de novo whole-genome sequences of the 13 strains tested in this study have been recently obtained with long-read sequencing technology (Ramírez-Sánchez et al. 2022). Comparative genomics, notably for their pathogen-associated molecular pattern sequences (i.e., flagellin, EF-TU), may bring very informative data on their potential recognition by *A. thaliana*, thereby making an ecologically relevant link between microbiota recognition and plant innate immunity in the leaf compartment.

Data availability statement. Raw phenotypic data are available in Supplementary Data Set 1.

ACKNOWLEDGMENTS

We are grateful to the members of the ECOGEN team for their assistance during the sowing and thinning.

LITERATURE CITED

Aoun, N., Desaint, H., Boyrie, L., Bonhomme, M., Deslandes, L., Berthomé, R., and Roux, F. 2020. A complex network of additive and epistatic quantitative trait loci underlies natural variation of *Arabidopsis thaliana* quantitative disease resistance to *Ralstonia solanacearum* under heat stress. Mol. Plant Pathol. 21:1405-1420.

Aoun, N., Tauleigne, L., Lonjon, F., Deslandes, L., Vailleau, F., Roux, F., and Berthomé, R. 2017. Quantitative disease resistance under elevated temperature: Genetic basis of new resistance mechanisms to *Ralstonia solanacearum*. Front. Plant Sci. 8:1387.

Badet, T., Voisin, D., Mbengue, M., Barascud, M., Sucher, J., Sadon, P., Balagué, C., Roby, D., and Raffaele, S. 2017. Parallel evolution of the *POQR* prolyl oligo peptidase gene conferring plant quantitative disease resistance. PLoS Genet. 13:e1007143.

Baekelandt, A., Pauwels, L., Wang, Z., Li, N., De Milde, L., Natran, A., Vermeersch, M., Li, Y., Goossens, A., Inzé, D., and Gonzalez, N. 2018. Arabidopsis leaf flatness is regulated by PPD2 and NINJA through repression of *CYCLIN D3* genes. Plant Physiol. 178:217-232.

Bai, B., Liu, W., Qiu, X., Zhang, J., Zhang, J., and Bai, Y. 2022. The root microbiome: Community assembly and its contributions to plant fitness. J. Integr. Plant Biol. 64:230-243.

Bartoli, C., Frachon, L., Barret, M., Rigal, M., Huard-Chauveau, C., Mayjonade, B., Zanchetta, C., Bouchez, O., Roby, D., Carrère, S., and Roux, F. 2018. In situ relationships between microbiota and potential pathobiota in *Arabidopsis thaliana*. ISME J. 12:2024-2038.

Bartoli, C., Rigal, M., Huard-Chauveau, C., Mayjonade, B., and Roux, F. 2024. The genetic architecture of the adaptive potential of *Arabidopsis thaliana* in response to *Pseudomonas syringae* strains isolated from south-west France. Plant Pathol. 73:884-897.

Bartoli, C., and Roux, F. 2017. Genome-wide association studies in plant pathosystems: Toward an ecological genomics approach. Front. Plant Sci. 8:763.

Bazin, J., Mariappan, K., Jiang, Y., Blein, T., Voelz, R., Crespi, M., and Hirt, H. 2020. Role of MPK4 in pathogen-associated molecular pattern-triggered alternative splicing in Arabidopsis. PLoS Pathog. 16:e1008401.

Bergelson, J., Brachi, B., Roux, F., and Vailleau, F. 2021. Assessing the potential to harness the microbiome through plant genetics. Curr. Opin. Biotechnol. 70:167-173.

Bergelson, J., and Roux, F. 2010. Towards identifying genes underlying ecologically relevant traits in *Arabidopsis thaliana*. Nat. Rev. Genet. 11:867-879.

Bonhomme, M., Fariello, M. I., Navier, H., Hajri, A., Badis, Y., Miteul, H., Samac, D. A., Dumas, B., Baranger, A., Jacquet, C., and Pilet-Nayel, M.-L. 2019. A local score approach improves GWAS resolution and detects minor QTL : Application to *Medicago truncatula* quantitative disease resistance to multiple *Aphanomyces euteiches* isolates. Heredity 123:517-531.

Bourdais, G., Burdiak, P., Gauthier, A., Nitsch, L., Salojärvi, J., Rayapuram, C., Idänheimo, N., Hunter, K., Kimura, S., Merilo, E., Vaattovaara, A., Oracz, K., Kaufholdt, D., Pallon, A., Anggoro, D. T., Glów, D., Lowe, J., Zhou, J., Mohammadi, O., Puukko, T., Albert, A., Lang, H., Ernst, D., Kollist, H., Brosché, M., Durner, J., Borst, J. W., Collinge, D. B., Karpiński, S., Lyngkjær, M. F., Robatzek, S., Wrzaczek, M., Kangasjärvi, J., and CRK Consortium. 2015. Large-scale phenomics identifies primary and fine-tuning roles for CRKs in responses related to oxidative stress. PLoS Genet. 11:e1005373.

Burdon, J. J., Thrall, P. H., and Ericson, L. 2006. The current and future dynamics of disease in plant communities. Annu. Rev. Phytopathol. 44:19-39.

Burdon, J. J., and Zhan, J. 2020. Climate change and disease in plant communities. PLoS Biol. 18:e3000949.

Chung, H. Y., and Sunter, G. 2014. Interaction between the transcription factor AtTIFY4B and begomovirus AL2 protein impacts pathogenicity. Plant Mol. Biol. 86:185-200.

Chung, K. P., Zeng, Y., Li, Y., Ji, C., Xia, Y., and Jiang, L. 2018. Signal motif-dependent ER export of Qc-SNARE BET12 interacts with MEMB12 and affects PR1 trafficking in *Arabidopsis*. J. Cell Sci. 131:jcs202838.

Colaianni, N. R., Parys, K., Lee, H.-S., Conway, J. M., Kim, N. H., Edelbacher, N., Mucyn, T. S., Madalinski, M., Law, T. F., Jones, C. D., Belkhadir, Y., and Dangl, J. L. 2021. A complex immune response to flagellin epitope variation in commensal communities. Cell Host Microbe 29:635-649.e9.

Cotta, M. S., do Amaral, F. P., Cruz, L. M., Wassem, R., de Oliveira Pedrosa, F., Yokoyama, T., and Stacey, G. 2020. Genome-wide association studies reveal important candidate genes for the *Bacillus pumilus* TUAT-1-*Arabidopsis thaliana* interaction. bioRxiv 117002.

Curtin, S. J., Tiffin, P., Guhlin, J., Trujillo, D. I., Burghardt, L. T., Atkins, P., Baltes, N. J., Denny, R., Voytas, D. F., Stupar, R. M., and Young, N. D. 2017. Validating genome-wide association candidates controlling quantitative variation in nodulation. Plant Physiol. 173:921-931.

Debieu, M., Huard-Chauveau, C., Genissel, A., Roux, F., and Roby, D. 2016. Quantitative disease resistance to the bacterial pathogen *Xanthomonas campestris* involves an Arabidopsis immune receptor pair and a gene of unknown function. Mol. Plant Pathol. 17:510-520.

Delplace, F., Huard-Chauveau, C., Dubiella, U., Khafif, M., Alvarez, E., Langin, G., Roux, F., Peyraud, R., and Roby, D. 2020. Robustness of plant quantitative disease resistance is provided by a decentralized immune network. Proc. Natl. Acad. Sci. U.S.A. 117:18099-18109.

Demirjian, C., Razavi, N., Desaint, H., Lonjon, F., Genin, S., Roux, F., Berthomé, R., and Vailleau, F. 2022. Study of natural diversity in response to a key pathogenicity regulator of *Ralstonia solanacearum* reveals new susceptibility genes in *Arabidopsis thaliana*. Mol. Plant Pathol. 23:321-338.

Demirjian, C., Razavi, N., Yu, G., Mayjonade, B., Zhang, L., Lonjon, F., Chardon, F., Carrere, S., Gouzy, J., Genin, S., Macho, A. P., Roux, F., Berthomé, R., and Vailleau, F. 2023a. An atypical *NLR* gene confers bacterial wilt susceptibility in *Arabidopsis*. Plant Commun. 4:100607.

Demirjian, C., Vailleau, F., Berthomé, R., and Roux, F. 2023b. Genome-wide association studies in plant pathosystems: Success or failure? Trends Plant Sci. 28:471-485.

Deng, Y., Ning, Y., Yang, D.-L., Zhai, K., Wang, G.-L., and He, Z. 2020. Molecular basis of disease resistance and perspectives on breeding strategies for resistance improvement in crops. Mol. Plant 13:1402-1419.

Duflos, R., Vailleau, F., and Roux, F. 2024. Toward ecologically relevant genetics of interactions between host plants and plant growth-promoting bacteria. Adv. Genet. https://doi.org/10.1002/ggn2.202300210

Frachon, L., Bartoli, C., Carrère, S., Bouchez, O., Chaubet, A., Gautier, M., Roby, D., and Roux, F. 2018. A genomic map of climate adaptation in *Arabidopsis thaliana* at a micro-geographic scale. Front. Plant Sci. 9:967.

Frachon, L., Libourel, C., Villoutreix, R., Carrère, S., Glorieux, C., Huard-Chauveau, C., Navascués, M., Gay, L., Vitalis, R., Baron, E., Amsellem, L., Bouchez, O., Vidal, M., Le Corre, V., Roby, D., Bergelson, J., and Roux, F. 2017. Intermediate degrees of synergistic pleiotropy drive adaptive evolution in ecological time. Nat. Ecol. Evol. 1:1551-1561.

Frachon, L., Mayjonade, B., Bartoli, C., Hautekèete, N.-C., and Roux, F. 2019. Adaptation to plant communities across the genome of *Arabidopsis thaliana*. Mol. Biol. Evol. 36:1442-1456.

Franciosini, A., Lombardi, B., Iafrate, S., Pecce, V., Mele, G., Lupacchini, L., Rinaldi, G., Kondou, Y., Gusmaroli, G., Aki, S., Tsuge, T., Deng, X.-W., Matsui, M., Vittorioso, P., Costantino, P., and Serino, G. 2013. The *Arabidopsis* COP9 SIGNALOSOME INTERACTING F-BOX KELCH 1 protein forms an SCF ubiquitin ligase and regulates hypocotyl elongation. Mol. Plant 6:1616-1629.

Friedman, E. J., Wang, H. X., Jiang, K., Perovic, I., Deshpande, A., Pochapsky, T. C., Temple, B. R. S., Hicks, S. N., Harden, T. K., and Jones, A. M. 2011.

Acireductone dioxygenase 1 (ARD1) is an effector of the heterotrimeric G protein β subunit in *Arabidopsis*. J. Biol. Chem. 286:30107-30118.

Guo, X., Li, L., Liu, X., Zhang, C., Yao, X., Xun, Z., Zhao, Z., Yan, W., Zou, Y., Liu, D., Li, H., and Lu, H. 2022. MYB2 is important for tapetal PCD and pollen development by directly activating protease expression in *Arabidopsis*. Int. J. Mol. Sci. 23:3563.

Gupta, P. K., Kulwal, P. L., and Jaiswal, V. 2019. Association mapping in plants in the post-GWAS genomics era. Adv. Genet. 104:75-154.

Huard-Chauveau, C., Perchepied, L., Debieu, M., Rivas, S., Kroj, T., Kars, I., Bergelson, J., Roux, F., and Roby, D. 2013. An atypical kinase under balancing selection confers broad-spectrum disease resistance in *Arabidopsis*. PLoS Genet. 9:e1003766.

Jeger, M. J. 2022. The impact of climate change on disease in wild plant populations and communities. Plant Pathol. 71:111-130.

Karasov, T. L., Kniskern, J. M., Gao, L., DeYoung, B. J., Ding, J., Dubiella, U., Lastra, R. O., Nallu, S., Roux, F., Innes, R. W., Barrett, L. G., Hudson, R. R., and Bergelson, J. 2014. The long-term maintenance of a resistance polymorphism through diffuse interactions. Nature 512:436-440.

Li, B., Wang, R., Wang, S., Zhang, J., and Chang, L. 2021. Diversified regulation of cytokinin levels and signaling during *Botrytis cinerea* infection in *Arabidopsis*. Front. Plant Sci. 12:584042.

Macho, A. P., and Zipfel, C. 2014. Plant PRRs and the activation of innate immune signaling. Mol. Cell 54:263-272.

Maier, B. A., Kiefer, P., Field, C. M., Hemmerle, L., Bortfeld-Miller, M., Emmenegger, B., Schäfer, M., Pfeilmeier, S., Sunagawa, S., Vogel, C. M., and Vorholt, J. A. 2021. A general non-self response as part of plant immunity. Nat. Plants 7:696-705.

Mantelin, S., and Touraine, B. 2004. Plant growth-promoting bacteria and nitrate availability: Impacts on root development and nitrate uptake. J. Exp. Bot. 55:27-34.

Monaghan, J., and Zipfel, C. 2012. Plant pattern recognition receptor complexes at the plasma membrane. Curr. Opin. Plant Biol. 15:349-357.

Naitam, M., Kaushik, R., and Sharma, A. 2021. Crop microbiome engineering and relevance in abiotic stress tolerance. Pages 253-277 in: Climate Change and the Microbiome: Sustenance of the Ecosphere. D. K. Choudhary, A. Mishra, and A. Varma, eds. Springer, Cham, Switzerland.

Parys, K., Colaianni, N. R., Lee, H.-S., Hohmann, U., Edelbacher, N., Trgovcevic, A., Blahovska, Z., Lee, D., Mechtler, A., Muhari-Portik, Z., Madalinski, M., Schandry, N., Rodríguez-Arévalo, I., Becker, C., Sonnleitner, E., Korte, A., Bläsi, U., Geldner, N., Hothorn, M., Jones, C. D., Dangl, J. L., and Belkhadir, Y. 2021. Signatures of antagonistic pleiotropy in a bacterial flagellin epitope. Cell Host Microbe 29:620-634.e9.

Pfeilmeier, S., Petti, G. C., Bortfeld-Miller, M., Daniel, B., Field, C. M., Sunagawa, S., and Vorholt, J. A. 2021. The plant NADPH oxidase RBOHD is required for microbiota homeostasis in leaves. Nat. Microbiol. 6:852-864.

Ramírez-Sánchez, D., Gibelin-Viala, C., Mayjonade, B., Duflos, R., Belmonte, E., Pailler, V., Bartoli, C., Carrere, S., Vailleau, F., and Roux, F. 2022. Investigating genetic diversity within the most abundant and prevalent non-pathogenic leaf-associated bacteria interacting with *Arabidopsis thaliana* in natural habitats. Front. Microbiol. 13:984832.

Ramírez-Sánchez, D., Gibelin-Viala, C., Roux, F., and Vailleau, F. 2023. Genetic architecture of the response of *Arabidopsis thaliana* to a native plant-growth-promoting bacterial strain. Front. Plant Sci. 14:1266032.

Ristaino, J. B., Anderson, P. K., Bebber, D. P., Brauman, K. A., Cunniffe, N. J., Fedoroff, N. V., Finegold, C., Garrett, K. A., Gilligan, C. A., Jones, C. M., Martin, M. D., MacDonald, G. K., Neenan, P., Records, A., Schmale, D. G., Tateosian, L., and Wei, Q. 2021. The persistent threat of emerging plant disease pandemics to global food security. Proc. Natl. Acad. Sci. U.S.A. 118:e2022239118.

Roux, F., and Frachon, L. 2022. A genome-wide association study in *Arabidopsis thaliana* to decipher the adaptive genetics of quantitative disease resistance in a native heterogeneous environment. PLoS One 17: e0274561.

Roux, F., Frachon, L., and Bartoli, C. 2023. The genetic architecture of adaptation to leaf and root bacterial microbiota in *Arabidopsis thaliana*. Mol. Biol. Evol. 40:msad093.

Roux, F., Mary-Huard, T., Barillot, E., Wenes, E., Botran, L., Durand, S., Villoutreix, R., Martin-Magniette, M.-L., Camilleri, C., and Budar, F. 2016. Cytonuclear interactions affect adaptive traits of the annual plant *Arabidopsis thaliana* in the field. Proc. Natl. Acad. Sci. U.S.A. 113:3687-3692.

Roux, F., Voisin, D., Badet, T., Balagué, C., Barlet, X., Huard-Chauveau, C., Roby, D., and Raffaele, S. 2014. Resistance to phytopathogens *e tutti quanti*: Placing plant quantitative disease resistance on the map. Mol. Plant Pathol. 15:427-432.

Savary, S., Willocquet, L., Pethybridge, S. J., Esker, P., McRoberts, N., and Nelson, A. 2019. The global burden of pathogens and pests on major food crops. Nat. Ecol. Evol. 3:430-439.

Stanton-Geddes, J., Paape, T., Epstein, B., Briskine, R., Yoder, J., Mudge, J., Bharti, A. K., Farmer, A. D., Zhou, P., Denny, R., May, G. D., Erlandson, S., Yakub, M., Sugawara, M., Sadowsky, M. J., Young, N. D., and Tiffin, P. 2013. Candidate genes and genetic architecture of symbiotic and agronomic traits revealed by whole-genome, sequence-based association genetics in *Medicago truncatula*. PLoS One 8:e65688.

Torkamaneh, D., Chalifour, F.-P., Beauchamp, C. J., Agrama, H., Boahen, S., Maaroufi, H., Rajcan, I., and Belzile, F. 2020. Genome-wide association analyses reveal the genetic basis of biomass accumulation under symbiotic nitrogen fixation in African soybean. Theor. Appl. Genet. 133:665-676.

Trivedi, P., Leach, J. E., Tringe, S. G., Sa, T., and Singh, B. K. 2020. Plant-microbiome interactions: From community assembly to plant health. Nat. Rev. Microbiol. 18:607-621.

Vidotti, M. S., Lyra, D. H., Morosini, J. S., Granato, Í. S. C., Quecine, M. C., de Azevedo, J. L., and Fritsche-Neto, R. 2019. Additive and heterozygous (dis)advantage GWAS models reveal candidate genes involved in the genotypic variation of maize hybrids to *Azospirillum brasilense*. PLoS One 14:e0222788.

Vorholt, J. A. 2012. Microbial life in the phyllosphere. Nat. Rev. Microbiol. 10:828-840.

Wang, M., Roux, F., Bartoli, C., Huard-Chauveau, C., Meyer, C., Lee, H., Roby, D., McPeek, M. S., and Bergelson, J. 2018. Two-way mixed-effects methods for joint association analysis using both host and pathogen genomes. Proc. Natl. Acad. Sci. U.S.A. 115:E5440-E5449.

Watanabe, E., Mano, S., Nishimura, M., and Yamada, K. 2019. AtUBL5 regulates growth and development through pre-mRNA splicing in *Arabidopsis thaliana*. PLoS One 14:e0224795.

White, D. W. R. 2022. PEAPOD repressors modulate and coordinate developmental responses to light intensity in *Arabidopsis*. New Phytol. 235:1470-1485.

Wintermans, P. C. A., Bakker, P. A. H. M., and Pieterse, C. M. J. 2016. Natural genetic variation in *Arabidopsis* for responsiveness to plant growth-promoting rhizobacteria. Plant Mol. Biol. 90:623-634.

Yang, W., Choi, M.-H., Noh, B., and Noh, Y.-S. 2020. De novo shoot regeneration controlled by HEN1 and TCP3/4 in *Arabidopsis*. Plant Cell Physiol. 61:1600-1613.

Yeh, Y.-H., Chang, Y.-H., Huang, P.-Y., Huang, J.-B., and Zimmerli, L. 2015. Enhanced *Arabidopsis* pattern-triggered immunity by overexpression of cysteine-rich receptor-like kinases. Front. Plant Sci. 6:322.

Zhan, J., Ericson, L., González-Jiménez, J., and Burdon, J. J. 2022. Disease influences host population growth rates in a natural wild plant–pathogen association over a 30-year period. J. Ecol. 110:173-184.

Zhang, Y., Fan, S., Hua, C., Teo, Z. W. N., Kiang, J. X., Shen, L., and Yu, H. 2022. Phase separation of HRLP regulates flowering time in *Arabidopsis*. Sci. Adv. 8:eabn5488.